IOP Publishing Journal of Physics D: Applied Physics

J. Phys. D: Appl. Phys. **47** (2014) 485501 (13pp) doi:10.1088/0022-3727/47/48/485501

Evaluation of the optoelectronic properties and corrosion behavior of Al_2O_3-doped ZnO films prepared by dc pulsed magnetron sputtering

C Zubizarreta[1], E G Berasategui[1], R Bayón[1], R Escobar Galindo[2,4], R Barros[3], D Gaspar[3], D Nunes[3], T Calmeiro[3], R Martins[3], E Fortunato[3] and J Barriga[1]

[1] IK4-TEKNIKER, Polo Tecnológico de Eibar, c/ Iñaki Goenaga, 5, 20600 Eibar, Spain
[2] Instituto de Ciencia de Materiales de Madrid (ICMM -CSIC), Cantoblanco, 28049 Madrid, Spain
[3] CENIMAT/I3N, Departamento de Ciências dos Materiais, Faculdade de Ciências e Tecnologia, Universidade Nova de Lisboa, 2829-516 Caparica, Portugal

E-mail: cristina.zubizarreta@tekniker.es

Received 20 June 2014, revised 23 September 2014
Accepted for publication 7 October 2014
Published 13 November 2014

Abstract

The main requirements for transparent conducting oxide (TCO) films acting as electrodes are a high transmission rate in the visible spectral region and low resistivity. However, in many cases, tolerance to temperature and humidity exposure is also an important requirement to be fulfilled by the TCOs to assure proper operation and durability. Besides improving current encapsulation methods, the corrosion resistance of the developed TCOs must also be enhanced to warrant the performance of optoelectronic devices.

In this paper the performance of aluminum-doped zinc oxide (AZO) films deposited by pulsed dc magnetron sputtering has been studied. Structure, optical transmittance/reflectance, electrical properties (resistivity, carrier concentration and mobility) and corrosion resistance of the developed coatings have been analyzed as a function of the doping of the target and the coating thickness. Films grown from a 2.0 wt% Al_2O_3 target with a thickness of approximately 1 μm showed a very low resistivity of 6.54 $\times$ 10^{-4} Ωcm and a high optical transmittance in the visible range of 84%. Corrosion studies of the developed samples have shown very low corrosion currents (nanoamperes), very high corrosion resistances (in the order of 10^7 Ω) and very high electrochemical stability, indicating no tendency for electrochemical corrosion degradation.

Keywords: AZO, PVD, electrochemical impedance, polarization, optoelectronics

(Some figures may appear in colour only in the online journal)

1. Introduction

Transparent conductive oxides (TCOs) have attracted great attention in a wide variety of applications where high transmittance in the visible range and low resistivity are necessary. The actual and potential applications of TCO thin films include flat panel displays, photovoltaic cells, low emissivity windows, electrochromic windows, transparent thin film transistors, light-emitting diodes and semiconductor lasers.

When the applications entail long-term environmental exposure, the performance of the devices deteriorates, diminishing their reliability. TCO acting as an electrode is one of

[4] Author to whom any correspondence should be addressed. Abengoa Research, Energia Solar 1, Palmas Altas, Seville 41014, Spain

the most exposed materials in the different stacks. To warranty the performance of these layers, not only are the optoelectronic properties important; durability must also be ensured. The degradation rate of this layer is influenced by factors such as film thickness, deposition conditions and exposure history [1]. To our knowledge, there is little literature on this topic [2–4]. Thus, more research is needed in order to improve its corrosion resistance.

Among the different TCOs, aluminum-doped zinc oxide (AZO) has been recognized in recent years as a potential replacement for commercial indium-tin-oxide and fluorine-doped tin-oxide. It has good optical and electrical properties [5, 6] and other advantages such as its non-toxicity and high thermal and chemical stability, associated with low cost and resource availability [7].

AZO coatings can be prepared by different deposition techniques, including dc magnetron sputtering (MS [8]), RF MS [9–11], pulsed dc MS [12, 13], pulsed laser deposition [14], reactive MS [15, 16], vacuum arc plasma evaporation [17] and sol-gel [18], among others. Pulsed dc MS presents high sputtering yields with high plasma density, long-term process stability, enhanced dynamic deposition rates [12, 19], and improved deposition speed and film quality [20]. These excellent properties make it the most attractive technology for commercial needs, being suitable for large-scale deposition of high-quality films at low temperature and being suitable for use on polymeric substrates [21, 22]. Nevertheless, in order to optimize the deposition process and the films obtained, in-depth research is required so as to understand the influence of growth conditions on the structure and optoelectronic properties of the coatings.

In the present paper, a thorough study of the influence of two different process parameters (Al_2O_3 doping and film thickness through deposition time) on the optoelectronic properties and the corrosion behavior of the developed layers has been carried out.

2. Experimental

The AZO coatings were deposited using the pulsed dc MS method, a type of physical vapor deposition (PVD) technique, using the industrial MIDAS 450 equipment developed by IK4-TEKNIKER. This system has three rectangular unbalanced magnetron evaporators of 550 × 125 mm target size that are magnetically linked with the help of a dummy magnet to form a closed field configuration. The distance between the evaporator and substrate was 120 mm, the substrates were rotating planetarily in a double rotation in a 400 mm diameter substrate holder at 8 rpm. Two different AZO ceramic targets ($ZnO:Al_2O_3$, 99.5:0.5 wt% and $ZnO:Al_2O_3$, 98:2.0 wt%) were used for the sputtering depositions. An argon pressure of 3×10^{-3} mbar was applied for all the experiments. The power level used to investigate the mechanism of AZO thin film growth was 2.9 W cm^{-2} corresponding to 2,000 W. The substrates were heated by means of industrial heaters up to a temperature of 350°C. The power source was dual-output pulsed dc (5–350 kHz) from AEI Pinnacle Plus + 5/5 kW. The duty cycle (4%) and the frequency (100 kHz) were fixed in all the processes. Films with different thicknesses (150, 310, 710 and 1,025 nm) were deposited. The samples were deposited on microscope slides (Menzel-Gläser) and on silicon wafers.

Table 1. Chemical composition obtained by RBS measurements of the coatings grown from different dopant concentrations (0.5 wt% and 2.0 wt% Al_2O_3) in the target.

Sample	Zn (at%)	O (at%)	Al (at%)
AZO_0.5% Al_2O_3	47.5	50.1	2.4
AZO_2.0% Al_2O_3	45.7	50.6	3.7

The structural analysis of the samples was performed by x-ray diffraction (XRD; PANalytical, X'Pert Pro model) in grazing incidence geometry with Cu Kα line radiation (λ = 1.5406 Å) at room temperature.

In order to analyze the chemical composition of the coatings, Rutherford backscattering spectroscopy (RBS) was carried out. RBS experiments were performed with a 5 MV HVEE Tandetron [23], and the spectra were collected using 3.035 MeV He^+ ions at an ion dose of 10 μC. The data were acquired with a silicon surface barrier detector located at a scattering angle of 170°, and with an energy resolution of 20 keV. The experimental spectra were fitted with the software programs RBX [24] and SIMNRA [25].

Hall effect measurements at room temperature were used to determine the resistivity, the carrier concentration and the mobility of the majority carriers with a Bio-Rad HL5500 instrument.

The total (direct and diffuse) optical transmittance and the specular reflectance were measured in the wavelength range from 200 to 2,500 nm on microscope slides (Menzel-Gläser) 76 × 26 mm^2 in size using a Perkin-Elmer Lambda 950 spectrophotometer equipped with a 150 mm diameter integrating sphere.

Atomic force microscopy (AFM; Asylum Research MFP-3D Stand Alone) together with scanning electron microscopy (SEM/FIB, Zeiss Auriga Crossbeam microscope) revealed the roughness (Sq, in nm) and microstructure of the films.

Corrosion behavior of AZO-coated silicon wafers was studied by means of electrochemical impedance spectroscopy and polarization techniques. Coatings from targets with different Al_2O_3 dopant concentrations and different resultant thicknesses were evaluated. The measurements were performed in a three-electrode electrochemical cell using an Ag/AgCl (KCl 3M) reference electrode (SSC) and a platinum wire counter electrode. Tests were carried out at room temperature and under aerated conditions on an exposed area of 1 cm^2.

For simulating the corrosive media a solution of NaCl 0.06 M was used. Despite the fact that in many applications TCOs should work under acid or alkaline environments, a neutral and standard solution of NaCl was selected for this preliminary electrochemical characterization. Further studies in aqueous media under different pH values will be performed in the future when suitable deposition process parameters are selected according to preliminary characterization studies.

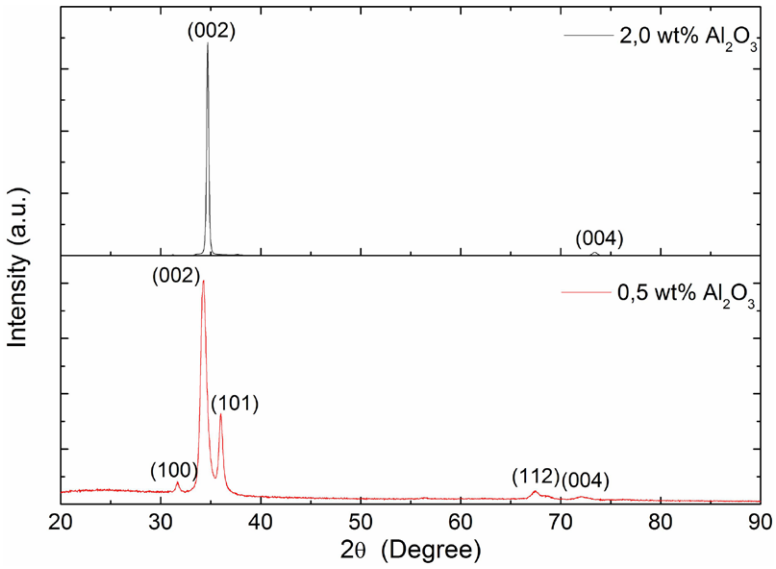

Figure 1. XRD diffractograms of the AZO thin films as a function of the Al_2O_3 concentration.

The procedure for evaluating the electrochemical response of the coatings doped with different aluminum content and grown with different thicknesses consisted of the measurement of the open circuit potential for 1,800 s of immersion in NaCl 0.06 M solution. After this time, electrochemical impedance spectroscopy was performed with a sinusoidal ac perturbation of ±10 mV amplitude at a frequency range from 10 kHz to 10 mHz, 10 freq/decade. The impedance spectra were registered at open circuit potential. After the impedance measurements, a potentiodynamic polarization curve was registered on each surface from –0.4 to 1.2 V (versus open circuit potential) at a scan rate of 0.5 mV s^{-1}. All potentials are referred to the Ag/AgCl electrode (0.207 V versus the standard hydrogen electrode).

3. Results and discussion

3.1. Influence of target doping

The effect of target doping on the electrical and optical properties of the AZO layers has been investigated considering two distinct Al_2O_3 concentrations, where ZnO targets with 0.5 wt% Al_2O_3 and 2.0 wt% Al_2O_3 concentrations have been evaluated, leading to thickness samples of 1,025 nm. From the previous studies, the argon pressure of 3×10^{-3} mbar has been established as the optimum parameter and has been employed for all the experiments [26].

As the first step, the composition and structure of the deposited coatings were analyzed. Table 1 shows the chemical composition obtained from RBS measurements of the coatings grown from targets with different dopant concentrations. Both samples are practically stoichiometric (oxygen content ~50 at%). Also, in both cases, the Al content in the AZO films is higher than the nominal one in the target, which was already reported in previous studies such as [27]. The sample prepared from a target with 0.5 wt% Al_2O_3 has 2.4 at% Al in the coating compared to 3.7 at% Al in the sample prepared from a target doped with 2.0 wt% Al_2O_3.

Table 2. Full width at half maximum (FWHM) of the (002) peak and grain size for the two Al_2O_3 dopant concentrations in the target, 0.5 wt% and 2.0 wt%.

[Al_2O_3] (wt%)	FWHM (rad.)	Grain size XRD (nm)
0.5	0.01074	14.1
2.0	0.00350	43.3

Table 3. Electrical resistivity (ρ), Hall mobility (μ) and carrier concentration (n) values for the ZnO targets with 2.0 wt% Al_2O_3 and 0.5 wt% Al_2O_3 concentrations.

Target doping	Resistivity (Ωcm)	Hall mobility (cm^2/Vs)	Carrier concentration (cm^{-3})
0.5 wt% Al_2O_3	2.07×10^{-3}	13.8	2.18×10^{20}
2.0 wt% Al_2O_3	6.54×10^{-4}	20.7	4.61×10^{20}

Figure 1 shows the x-ray diffraction patterns for both studied conditions. When the ZnO films are doped with Al_2O_3, Al^{3+} ions become part of the ZnO lattice in the substitutional sites of Zn^{2+} ions, and there may also be Al interstitial atoms. Both analyzed samples show the strong ZnO (002) peak of hexagonal wurtzite-type structure and also the (004) peak with very weak intensity. This indicates that the films grew along the *c*-axis orientation, perpendicular to the substrates. Thus, Al^{3+} ions substituting Zn^{2+} did not change the ZnO hexagonal wurtzite structure. No other phases, such as Al or Al_2O_3, were detected in the films.

For the 0.5 wt% Al_2O_3 concentration (101), (112) and (100) peaks are also shown, indicating that for lower dopant content there is a poorer *c*-axis orientation.

In addition to the *c*-axis orientation, a small shift of the peak position of the (002) plane is observed to a higher position when increasing the Al content in the film (from 34.28° for 0.5 wt% Al_2O_3 to 34.36° for 2.0 wt% Al_2O_3), which indicates

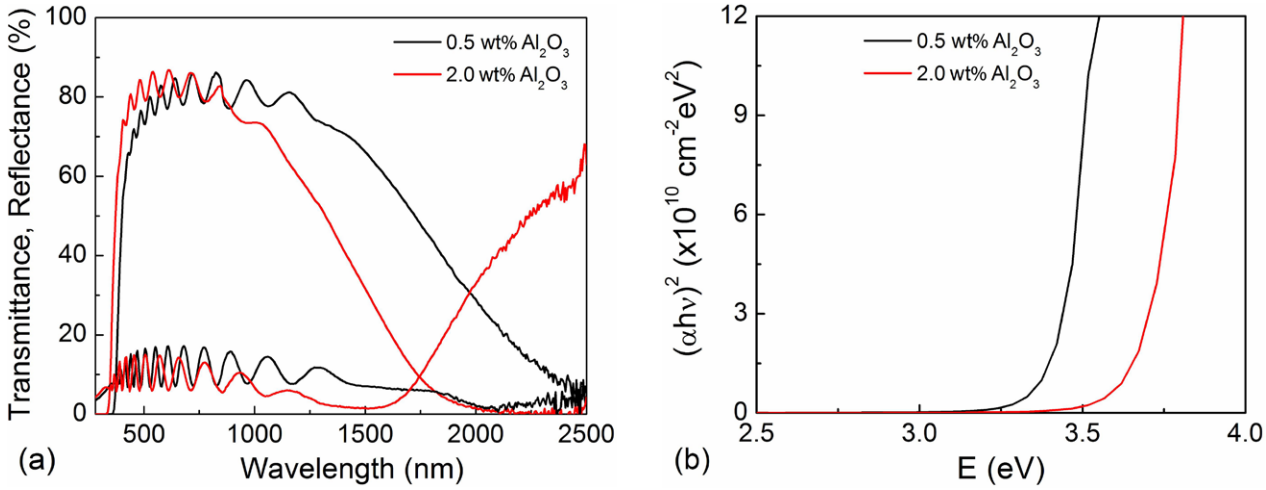

Figure 2. Optical properties of the AZO films obtained from targets with different dopant concentrations: (*a*) transmittance and reflectance spectra, (*b*) plot of $(\alpha h\nu)^2$ against photon energy ($h\nu$).

an increased influx of Al atoms at the Zn sites with increasing Al_2O_3 concentration [28].

For 0.5 wt% Al_2O_3 concentration, the (0 0 2) peak is slightly broader than for 2.0 wt%, indicating that the grain size of this film is smaller. The grain or crystallite size was obtained from the width of XRD peaks using Scherrer's formula [29]. As seen in table 2, the grain size of the films for 0.5 wt% Al_2O_3 concentration is 14.1 nm, and for the 2.0 wt% Al_2O_3 concentration it is 43.3 nm.

Table 3 shows the results from Hall measurements for the AZO films grown from targets with different Al_2O_3 concentrations. As the Al_2O_3 concentration of the target increases from 0.5 to 2.0 wt%, the resistivity decreases, reaching values of $6.54 \times 10^{-4}\,\Omega$cm. This decrease is due to an increase in carrier concentration and in Hall mobility, which can also be related to the higher Al content in the sample (table 1). The conduction characteristics of ZnO are basically dominated by electrons generated from oxygen vacancies and Zn interstitial atoms [30]. However, when the ZnO films are doped with Al_2O_3, the conductivity increases due to the contribution from Al^{3+} ions in the substitutional sites of Zn^{2+} ions and Al interstitial atoms as well as from oxygen vacancies and Zn interstitial atoms [27]. The bibliography indicates that there is a limit in doping concentration as the excess of Al atoms above a certain critical concentration in the ZnO films segregates into grain boundaries, decreasing the conductivity of the layer [27].

Correlating the electrical properties with the structural ones, the increase in resistivity for samples grown from the target with the lower dopant concentration could also be explained in terms of the segregation of Al content into the grain boundaries, since the grain boundaries increase with the decrease in grain size (table 2), which makes Al electrically inactive, causing this increase in resistivity [31].

The transmittance, reflectance and optical band gap for both samples have been measured and calculated (figure 2). Both films exhibit high optical transmittance in the visible wavelength range (84–86%). It is observed that the transmittance near the infrared region strongly decreases by increasing the amount of Al_2O_3 (2.0 wt%).

The decrease in transmittance in the near-infrared region corresponds to the increasing carrier density. This behavior is caused by the increase in plasma oscillation frequency with the increasing carrier density, which can be explained by the Drude theory and is well known in degenerated TCO films [32, 33].

The optical band gap, E_g, of a direct gap semiconductor can be determined by extrapolating the linear portion of $(\alpha h\nu)^2$ against the photon energy ($h\nu$ [34]), where α is the absorption coefficient. The band gap increases with the increase in the Al_2O_3 concentration, obtaining values of 3.41 eV for 0.5 wt% Al_2O_3 and values of 3.67 eV for 2.0 wt% Al_2O_3. This increase in the band gap is due to an increase in free electron concentration in the films as a result of Al doping. This shift of the band gap can be explained by the Burstein–Moss effect [35, 36], which suggests that a band gap can be widened with an increase in the carrier concentration. As the Fermi level moves up into the conduction band in an n-type semiconductor, the lower states in the conduction band get filled up, which means that more energy is required for the electrons to be excited from the valence band to the conduction band, leading to an extension of the optical band gap. Thus, the absorption edge shifts towards higher energy.

SEM and AFM analyses have been performed in order to determine the morphology of the deposited films regarding the variation in Al_2O_3 concentration, and the results are presented in figure 3. A columnar/polygon grain structure is clearly observed for the 0.5 wt% Al condition. Moreover, with the increase in Al_2O_3 concentration, a crater-like structure is evident, confirming that the dopant has a vital effect on the final film morphology [37]. The AFM measurements revealed maximum roughness values of approximately 23 and 21 nm for the 0.5 and 2.0 wt% Al_2O_3 doping conditions, respectively.

In summary, regarding the influence of the target dopant, it can be seen that although this parameter slightly affects the

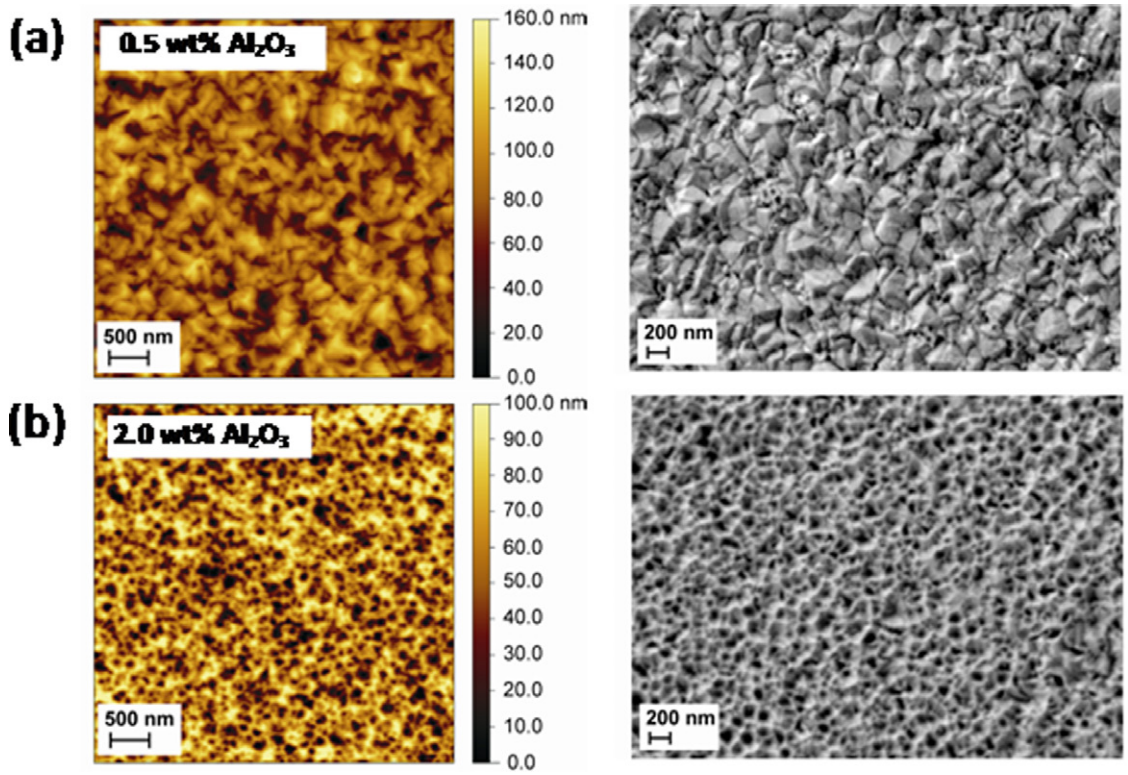

Figure 3. AFM and SEM images of the AZO films for the ZnO target with (*a*) 0.5 wt% Al_2O_3 and (*b*) 2.0 wt% Al_2O_3 concentrations.

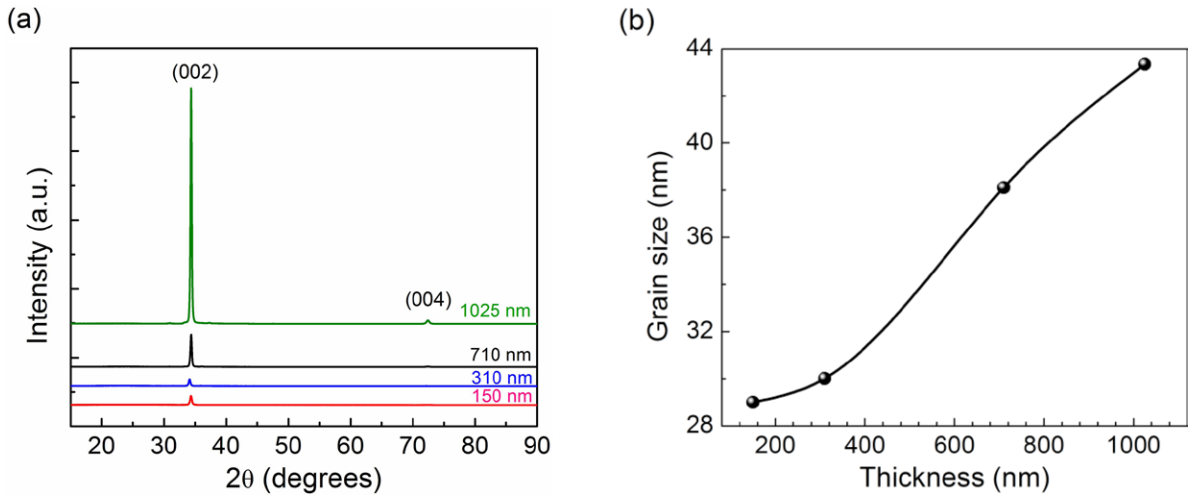

Figure 4. (*a*) XRD diffractograms and (*b*) grain size of the AZO thin films as a function of thickness.

optical properties in the visible region, the electrical properties are clearly improved using the target with a higher concentration of Al_2O_3.

3.2. Influence of coating thickness

To investigate the influence of coating thickness on the electrical and optical properties of the films, and taking into account the results obtained regarding the target dopant, AZO films of 150, 310, 710 and 1,025 nm thickness were deposited from a target of ZnO doped with 2.0 wt% Al_2O_3 under a pressure process of 3×10^{-3} mbar, a power of 2 kW and a pulse frequency of 100 kHz.

The XRD patterns of the AZO films with different thicknesses are shown in figure 4. It shows that the films obtained were polycrystalline with a hexagonal structure and highly oriented with the *c*-axis perpendicular to the substrate, having a Bragg peak along the (002) plane. All the samples also show the (004) peak with much less intensity, imperceptible in the figure for most of the samples.

For all the films studied, apparent peak shifts towards the low-angle side were observed compared to that of bulk ZnO ($2\theta = 34.45°$), which could indicate that stress exists in all the AZO films [38].

The surface and cross-section morphologies are presented in figure 5 for the various AZO film thicknesses studied. As

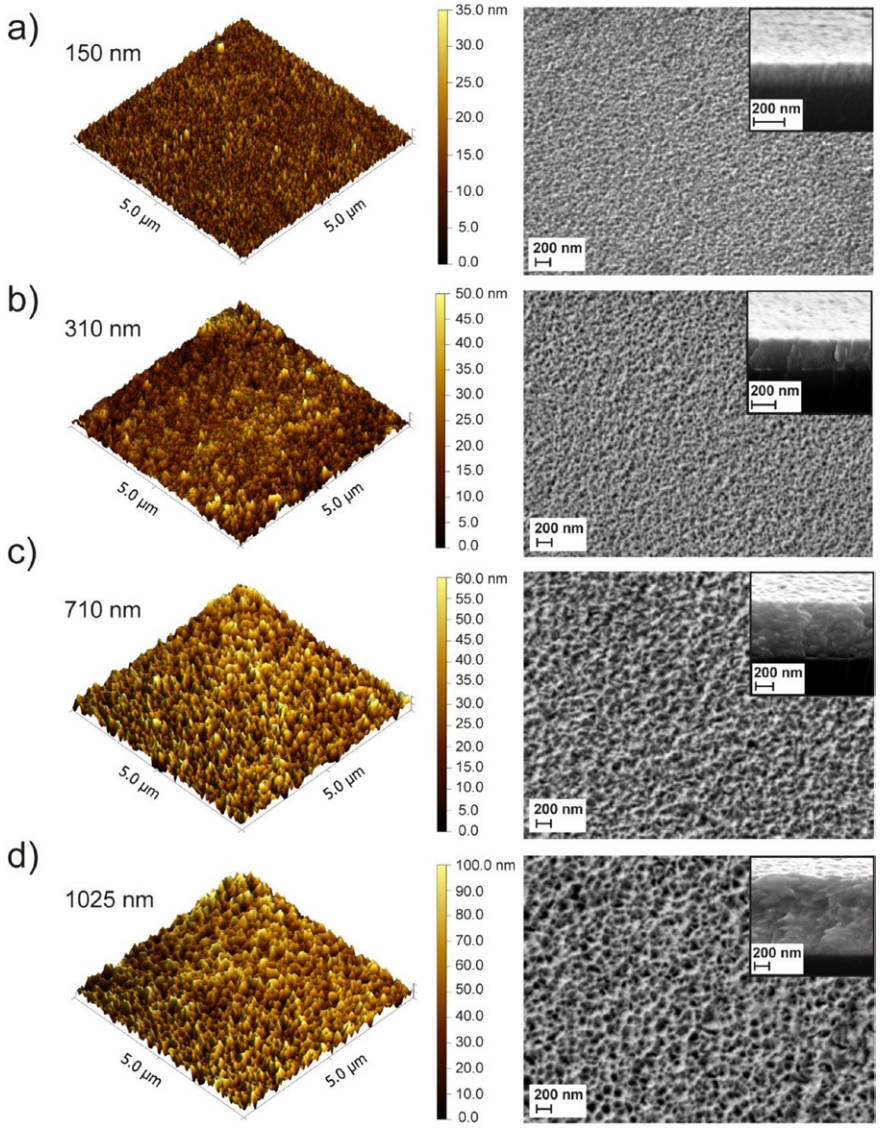

Figure 5. AFM and SEM images of the AZO films with (*a*) 150 nm, (*b*) 310 nm, (*c*) 710 nm and (*d*) 1,025 nm thickness.

expected [39], when the film thickness increases, the crystallinity is also increased, with evident enlargement in the crystallite size (figure 5). This tendency was confirmed by SEM images, with a clear increase in grain size related to the evolution of the film thickness. Moreover, AFM measurements also showed this behavior, reaching a maximum roughness value of approximately 21 nm (figure 6).

A nanocrystalline structure is clearly seen for the AZO films with lower thicknesses [40]. Moreover, the cross-section morphologies of these lower thickness conditions exhibited a columnar structure perpendicular to the substrates. The fine-scaled grains grow with deposition time, forming V-shaped structured grains. During the initial stages of deposition, random orientation nuclei were formed, and later the nanocrystalline structures engaged into a competitive growth stage, where crystals with higher vertical growth rate form large and well-oriented V-shaped grains [40]. This specific grain shape has been largely reported for ZnO:Al films subjected to etching processes [40–42], which may indicate that

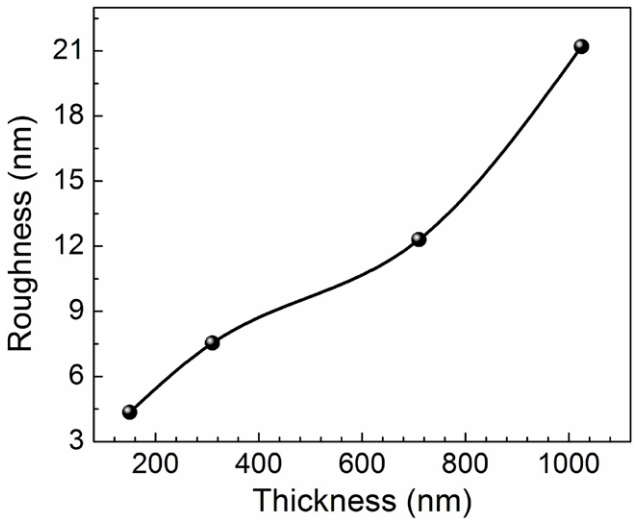

Figure 6. Roughness for AZO films as a function of thickness. (roughness mean square, RMS)

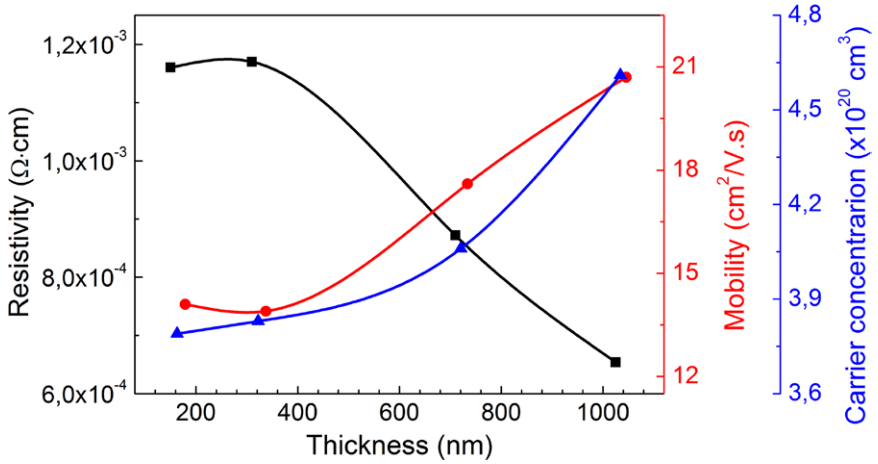

Figure 7. Variation of resistivity (■), Hall mobility (●) and carrier concentration (▲) as a function of thickness.

a similar process may be occurring during the film deposition for longer deposition times.

As previously mentioned, from figures 5(*a*)–(*d*), it is clear that the increase in film thickness resulted in a coarsening and roughening of the films; however, the columnar bulk structure observed at the lower thickness conditions evolves into a dense and heterogeneous structure. Moreover, a uniform distribution of grains can be observed for all the conditions studied.

Figure 7 shows the resistivity, Hall mobility and carrier concentration of the AZO as a function of the thickness. The lowest resistivity, obtained for the sample with the highest thickness (1,025 nm) is $6.54 \times 10^{-4} \Omega$cm. For thinner samples (150 and 310 nm) the electrical properties are very similar (almost identical) but for higher thicknesses the conductivity increases significantly (58% when increasing the thickness to 710 nm and 42% for the thickest layer of 1,025 nm).

This decrease in resistivity with the thickness is related to an increase in carrier concentration and in carrier mobility. Usually, as the thickness decreases the crystallinity of the layers worsens, having many defects due to large stress, and many free electrons can be caught by the large number of traps formed by these defects. Longer sputtering times (i.e. thicker coatings) entail higher temperatures on the substrate due to the ion bombardments. This effect increases the diffusion mobility of the sputtered particles, improving crystallinity and crystal size. Thus, the number of grain boundaries (scattering centers for free carriers) decrease, improving electrical properties [39].

Figure 8 shows the optical transmittance and the specular reflectance spectra of the AZO films deposited with different thicknesses. The average optical transmittance in the visible range (400–800 nm) was above 84% for all the films. When increasing film thickness the mean transmittance decreases slightly, which may be caused by optical scattering arising from longer optical paths and also by changes in the carrier concentration [43]. The conduction electrons are important because they dominate the optical properties of the materials in the near-infrared wavelengths. As the thickness of the films increases, the transmittance in the near-infrared wavelength region decreased. As mentioned in the previous section, this is a consequence of the higher carrier absorption caused by the increased carrier concentration in thicker films [32]. The reflectance results from the interference effect in the air/TCO. The visible range of wavelengths (400–800 nm) basically consists of interference fringes due to the thin film thicknesses, and a mean reflectance between 10 and 15%. Above 1,500 nm the films reveal high reflectance, overlapping a low transmittance region. This phenomenon, i.e. the transition from high transmittance/low reflectance to high reflectance/low transmittance, can be attributed to the increase in carrier concentration observed.

The optical band gap of AZO films decreases gradually when increasing the thickness (from 3.76 eV for 150 nm to 3.67 eV for 1,025 nm). This behavior could indicate that apart from carrier concentration and mean crystallite size [44, 45], there are other parameters that affect the band gap energy shift, such as the residual stress in the films [46] and the merging of an impurity band into the conduction band which compensates the Burstein–Moss effect [44].

From figure 8(*c*), we can observe that the haze factor increases with the evolution in morphology and increase in thickness due to light deflection at the film/air interface as a consequence of surface roughness [47].

3.3. Corrosion behavior

3.3.1. Effect of target doping. The evolution of the open circuit potential with immersion time in NaCl 0.06 M electrolyte was studied for two coatings with different aluminum content. For both coated surfaces, the potential increases slightly and reaches a stable value after few minutes of immersion. After 1,800 s of immersion, the AZO coating with 0.5% of Al_2O_3 doping shows an open circuit potential of –0.024 V (versus Ag/AgCl); the AZO coating with higher aluminum content shows a nobler potential (0.135 V). The aluminum concentration in AZO structures influences the electrochemical potential of the samples in saline media. It is known that the structure and composition of PVD coatings strongly influence the electrochemical response of the total coating due to differences in the coating density, micro-defects, grain sizes, etc [48].

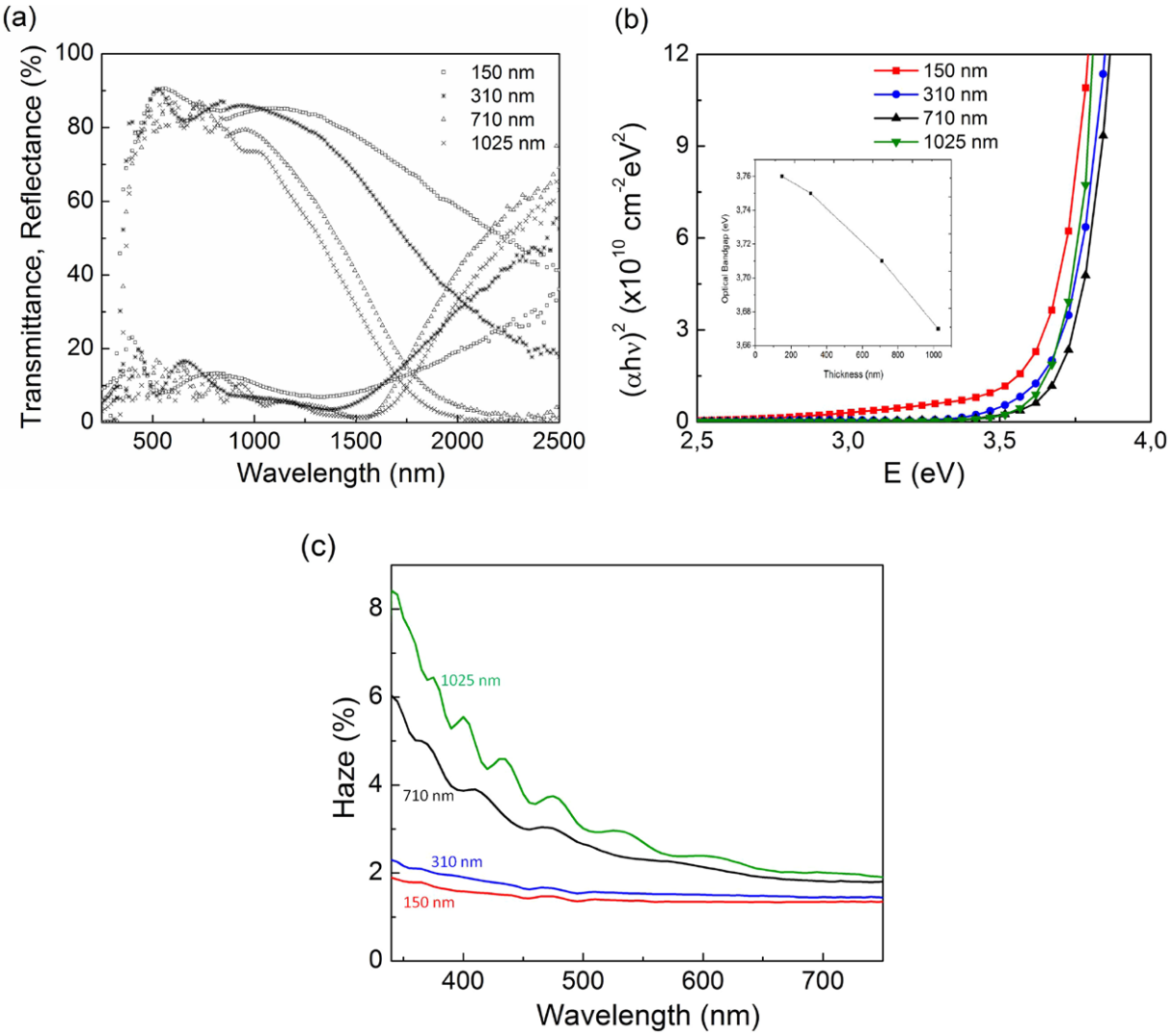

Figure 8. Optical behavior of AZO films of different thicknesses: (*a*) transmittance and reflectance spectra, (*b*) plot of $(\alpha h\nu)^2$ against photon energy ($h\nu$). The inset shows the optical band gap obtained by extrapolating the linear part, (*c*) haze factor.

After these 1,800 s of immersion in NaCl the open circuit potential was stable in both coatings. Then, electrochemical impedance spectroscopy was performed for each surface. It is well known that the impedance technique can be very useful for coating characterization because it provides information about the possible presence of pores and defects on their structure, and also about the system degradation with time. Figure 9 shows the Nyquist diagrams registered. Both coatings show similar curves reflecting an incomplete semi-circle. From the Bode diagrams of figure 9 it is easier to detect two time constants represented by two maximums in the *-Phase-f* curve and a shift in the slope of the $|Z|$-*f* curve in the medium frequency region (figure 10). Both AZO samples developed with different aluminum content presented very similar impedance diagrams and no significant differences in electrochemical response were found.

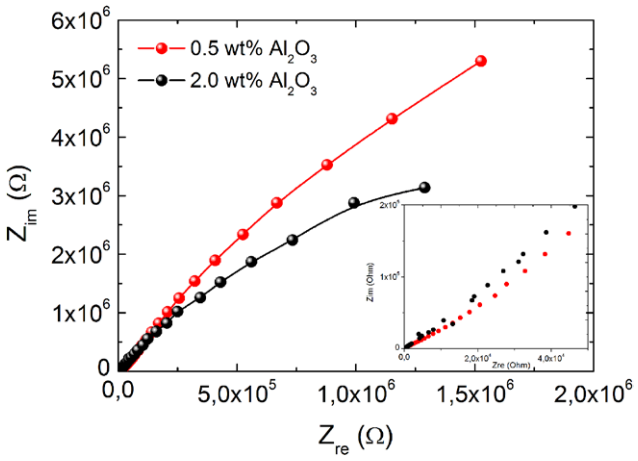

Figure 9. Nyquist diagram obtained from impedance measurements for AZO samples with different dopant concentrations.

Experimental data obtained by electrochemical impedance spectroscopy measurements were analyzed by means of an equivalent circuit composed of two time constants (figure 11). This circuit, composed of two pairs of constant phase element/resistance (CPR/R) elements combined in parallel is frequently employed to simulate the behavior of PVD coatings in aqueous media. At high frequencies, R1 is related to the resistance across the coating defects or pores

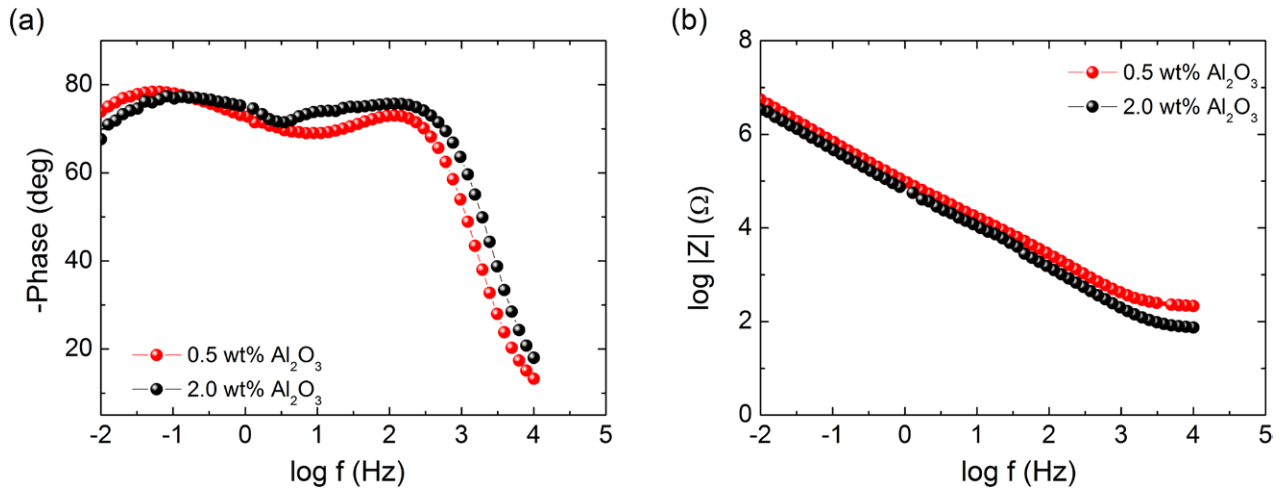

Figure 10. Bode plots of both coatings with different aluminum content.

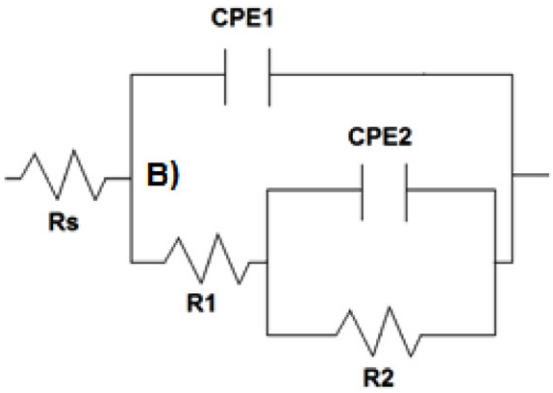

Figure 11. Equivalent circuit model used in the fitting process of experimental data.

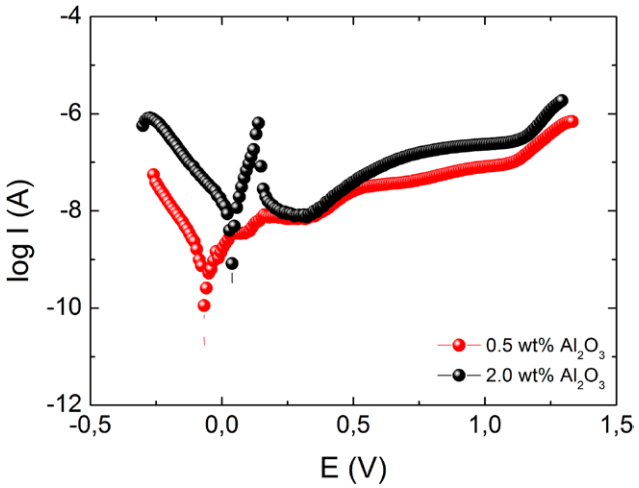

Figure 12. Polarization curves of AZO coatings in NaCl solution for AZO samples with different dopant concentrations (Al_2O_3 concentration in the target).

and CPE1 represents the capacitance of the coating (interface coating/electrolyte). In the second sub-circuit, R2 represents the corrosion resistance at the coating pores/defects bottom and CPE 2 the capacitance in the interface of the electrolyte/silicon substrate. Rs represents the resistance of the electrolyte. The impedance of the constant phase elements (CPE) is represented by the equation

$$Z_{CPE} = 1 / Y_0(i\omega)^n$$

where Y_0 is the admittance of an ideal capacitance and n is an empirical constant, ranging from 0 to 1. When $n = 1$, the CPE behaves as a pure capacitor and when $n = 0$, the constant phase element behaves as a pure resistor. Due to the high corrosion resistance of substrate by itself, some authors proposed an equivalent circuit with only one time constant to simulate the system [53]. The passive state of the silicon substrate at the bottom of the coating pores sometimes makes their contribution from the TCO coatings barely distinguishable.

At high frequencies (10^4 Hz), the angle phase registered in both coatings is close to 90°. Additionally, the low values of the Yo-CPE1 element (1.1×10^{-6} F cm^{-2} for 0.5 wt% Al_2O_3 and 1.6×10^{-6} F cm^{-2} for 2.0 wt% Al_2O_3) as well as the n-values close to 1 obtained in both coatings, suggest a capacitive behavior of the surface of both TCOs.

The corrosion resistance R1 was relatively higher in the case of the coating doped with 2.0 wt% Al_2O_3. The R1 values determined after fitting the experimental data were 44 kΩ for the 0.5 wt% Al_2O_3-doped coating and 74 kΩ for the 2.0 wt% Al_2O_3-doped coating. The second time constant detected in Bode plots appears at medium-low frequencies and is related to the electrochemical process taking place at the substrate/electrolyte interface across the coating defects or pores. In both cases the value of R2 is high enough, implying a low density of defects in both AZO coatings. Total corrosion resistance of coated systems taking into account R1 and R2 resistances is very high, in the order of $10^7 \Omega$. Comparing both coatings, the R2 value measured in the case of the 0.5 wt% Al_2O_3 dopant is approximately $8 \times 10^7 \Omega$, whereas the R2 value in the case of the sample with 2.0 wt% Al_2O_3 dopant is around $2 \times 10^7 \Omega$.

After impedance measurements, a potentiodynamic polarization test was additionally performed on coatings to evaluate their response in the anodic region and their respective corrosion currents. Figure 12 shows the curves obtained. Both

Table 4. Tafel analysis from polarization curve data for AZO samples with different dopant concentrations.

Target doping	E_{corr} (V)	I_{corr} (nA)	R_p (MΩ)	Corrosion rate (10^{-4} mm year^{-1})
2.0 wt% Al_2O_3	0.039	10.8	2.00	2.36
0.5 wt% Al_2O_3	–0.067	1.5	26.6	0.32

coatings coming from AZO targets with 2.0 and 0.5 wt% Al_2O_3 doping show a passive behavior in the anodic branch and very low corrosion currents (nanoamperes). Surface behavior is quite stable, especially for a potential range between 0.1 and 0.5 V, where the corrosion currents registered are lower than 10^{-8} A. At higher potentials, currents tend to increase slightly in both samples but always remain lower than 10^{-6} A, which suggests no electrochemical activity and passive response. Table 4 summarizes the kinetics parameters obtained by performing the corresponding Tafel analysis. The AZO coating with higher aluminum content starts to passivate at higher anodic potentials. At the beginning of the scan, the current increases, reaching values of approximately 10^{-6} A, but from 0.1 V the passive film starts to build up on its surface and the corrosion current decreases to 10^{-8} A and then, for higher potentials, remains lower than 10^{-6} A.

With regard to the Tafel analysis, lower aluminum content (corresponding to the coating obtained from the less doped target) seems to improve the corrosion resistance of the AZO. The corrosion current registered during the polarization process is always lower than that observed with the coating of higher aluminum content. The differences in both coatings should be related to the aluminum position in the microstructure of the coating. Samples with higher aluminum content and also with more electrically active aluminum have a higher tendency to react with oxygen.

The corrosion rates (mm/year) calculated from corrosion current values deduced from the Tafel analysis [49, 50] indicate greater durability for the coating with lower dopant. Samples with 0.5 wt% Al_2O_3 in the target show a corrosion rate of 3.2×10^{-5} mm year^{-1} whereas in the case of the coating with 2.0 wt% Al_2O_3 dopant this value increases to 2.4×10^{-4} mm year^{-1}.

3.3.2. Effect of coating thickness. The evolution of open circuit potential with immersion time in NaCl 0.06 M for AZO coatings with different thickness shows stable potential values with time for all the samples, indicating that passive aluminum and zinc oxide films have been formed and stabilized after a few seconds of contact with the electrolyte. After 1,800 s of immersion, the stabilized open circuit potential values for the coatings with increasing thickness were 0.063, 0.133, –0.096 and 0.135 V, respectively. Despite the fact that all surfaces exhibit very similar potential values, coatings of 310 and 1,025 nm thickness showed nobler potential than the rest. Differences in coating microstructures are reflected in corrosion tests by means of differences in the potential of equilibrium.

Nyquist diagrams registered from the electrochemical impedance spectroscopy carried out show incomplete

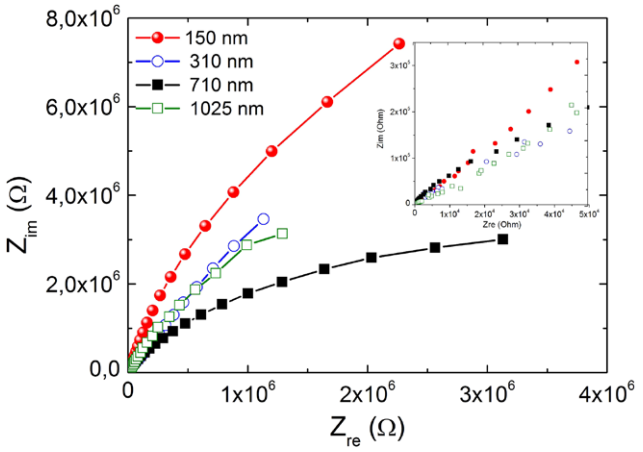

Figure 13. Nyquist diagram obtained from impedance measurements for AZO samples with different thicknesses.

semi-circular curves for all the coatings (figure 13). Bode diagrams in figure 14 show two maximums (time constants) in *-Phase-f* curves for all the samples, indicating the presence of pores and/or defects in the coatings, and as a consequence the contribution of the silicon substrate to the electrochemical measurement.

The experimental data registered for the four coatings could be fitted using the equivalent circuit depicted in figure 11 and previously discussed. The first time constant present at high frequencies with an angle phase close to 90° is related to the coatings' capacitive response as in previous tests on coatings with different aluminum content. In all cases, the value of Yo-CPE1 varies from 1.1–1.6 × 10^{-6} F cm^{-2}, the lowest value (1.1 × 10^{-6} F cm^{-2}) being related to the coatings with 150 and 310 nm thickness and the highest one to the coating with 1,025 nm thickness. The value of n1 was between 0.95 and 0.99 in all cases, which suggests a good capacitive response. At medium-low frequencies, the sample of 710 nm thickness shows a lower R2 value than the rest of the samples (8.5 × 10^6 Ω), which could indicate a higher pore or defect content or a diffusive process through the coating microstructure. Diffusional processes on PVD coatings are mainly related to the coating microstructure, which allows oxygen diffusion from the electrolyte to the substrate. Experimentally, this behavior can be clearly observed at low frequencies <10 mHz. Unfortunately, the impedance tests performed did not register the experimental data at such low frequency values. Theoretically, the impedance element for representing semi-infinite length Warburg diffusion is given by:

$$Z\omega = \sigma\omega^{1/2}(1 - i)$$

where σ is the Warburg coefficient and ω the frequency.

The Warburg impedance is an example of a constant phase element for which the phase angle is a constant 45° and the magnitude of the impedance ($|Z\omega| = \sigma\ 2^{1/2}/\omega^{1/2}$) is inversely proportional to the square root of the frequency ($1/\omega^{1/2}$) as a CPE element with an n-value of 0.5. In case of the coating with 710 nm thickness, the value of n2 measured was 0.66, which is closer to 0.5 (Warburg element) than a capacitor and

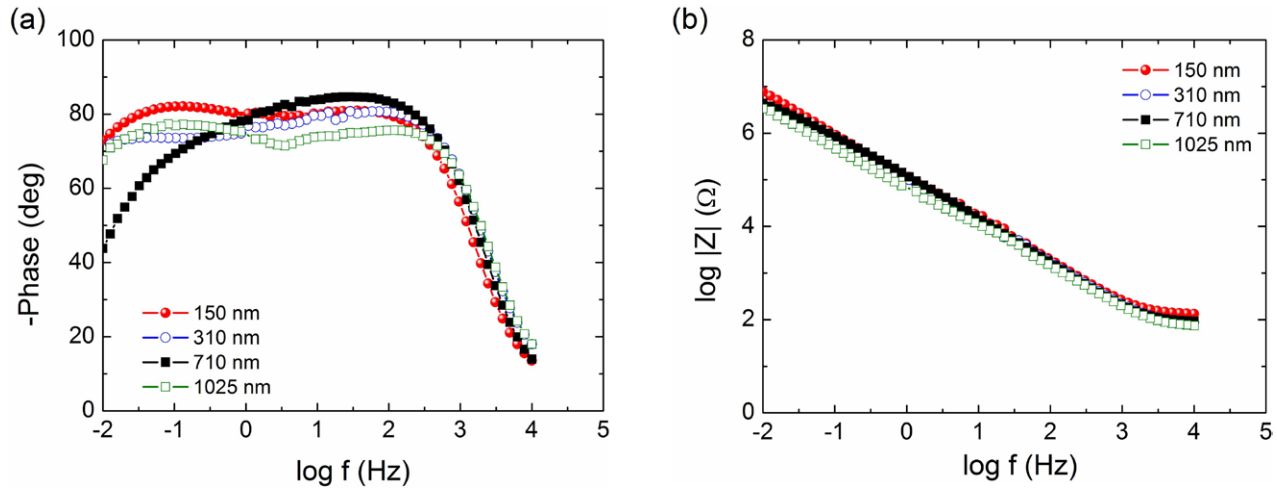

Figure 14. Bode plots of AZO coatings with different thicknesses.

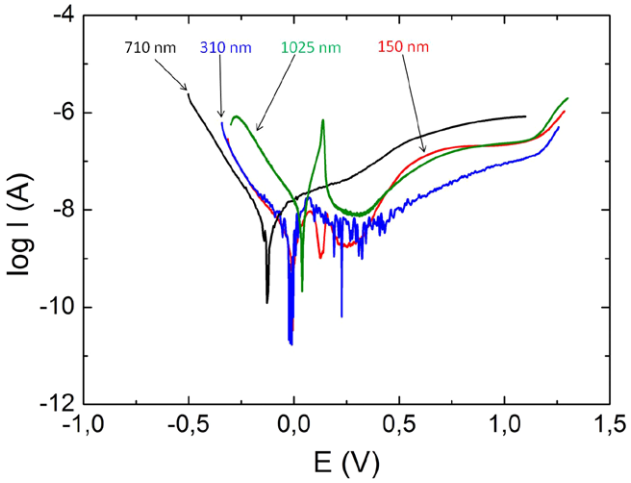

Figure 15. Polarization curves of AZO coatings in NaCl solution for AZO samples with different thicknesses.

thus the response of this coating at low frequencies may be related to oxygen diffusion through the coating structure. The Warburg coefficient can be expressed in terms of admittance as follows:

$$\sigma = 1/(Y_0 \cdot 2^{1/2})$$

Then, the magnitude of the impedance $|Z\omega|$ can be rewritten in terms of Y_0 being:

$$|Z\omega| = 1/Y_0\omega^{1/2} \text{ where } [Y_0] = \Omega^{-1}s^{1/2}$$

Low Y_0 values imply a high diffusion impedance ($Z\omega$) and high Warburg coefficient (σ). As the σ coefficient is inversely proportional to the diffusion coefficient D [52], then low Y_0-ω values imply a low diffusion coefficient, which is desirable to enhance the corrosion resistance of the coatings.

Comparing the corrosion resistances R1 and R2 calculated for the four coatings with different thicknesses, the following relation was found: 710 nm < 1,025 nm < 310 nm < 150 nm. The coating with the lowest thickness (150 nm) shows the highest corrosion resistance R2 (45 MΩ) followed by the coating with a thickness of 310 nm (42 MΩ). The tendency observed after the analysis of impedance measurements is that the electrochemical corrosion resistance depends on the coating thickness and lower thicknesses exhibit higher corrosion resistances.

Table 5. Tafel analysis from polarization curve data for AZO samples with different thicknesses.

Coating thickness (nm)	E_{corr} (V)	I_{corr} (nA)	R_p (MΩ)	Corrosion rate (10^{-4} mm year^{-1})
150	–0.005	3.8	9.2	1.10
310	–0.003	1.7	8.2	1.20
710	–0.132	7.2	6.0	2.90
1,025	0.039	10.8	2.0	2.36

The corrosion resistance test results of coatings deposited on silicon wafers with the method of potentiodynamic polarization curves in NaCl solution are presented in figure 15. It was found that, as a result of the electrochemical corrosion investigations, all the coatings deposited with different thicknesses present very high protection against corrosive agents such as chlorides.

Regardless of the thickness, all the coatings show a passive behavior in the anodic branch and very low corrosion currents (nanoamperes), which indicates a good protective effect. No pitting was detected in any case after reaching 1.5 V versus open circuit potential. Observing the potentiodynamic polarization curve analysis (table 5) and the corrosion rate data, the better corrosion resistance is shown by the thinner samples (150 and 310 nm thickness). Corrosion behavior could also be related to the surface roughness of the samples, as it has been reported in previous studies [51]. Samples with higher conductivity (figure 7) and higher roughness (figure 6), which correspond to the thickest coating, present lower corrosion resistance.

Summarizing the corrosion study carried out for the developed AZO coatings (with different dopant concentration and different thickness), all the samples have shown very good corrosion behavior (corrosion currents of nanoamperes and corrosion resistance in the order of $10^7\,\Omega$ in many cases).

Among the different samples, those with lower electrical conductivity have shown the higher corrosion performance. Specifically, the columnar/polygon structure related to the lower dopant concentration seems to induce better corrosion behavior (corrosion resistance of the order of $10^7\,\Omega$ and corrosion rate in NaCl 0.06 M of 0.32×10^{-4} mm year^{-1}). In any case, the corrosion results shown in this paper have simply been a part of a preliminary screening performed on AZO coatings in order to determine the most effective process conditions for developing the best AZO alternative, taking into account their ability to resist in a corrosive environment containing chlorides. Additionally, electrochemical tests in electrolytes with acid and alkaline pH as well as ageing (humidity and temperature cycles) tests specifically designed and standardized for the validation of these types of coatings, according to environmental corrosion requirements, will be fulfilled on selected surfaces developed under an optimized deposition process.

4. Conclusions

In summary, polycrystalline AZO layers with low resistivity and high transmission have been obtained by dc MS. The correlation between the process parameters (target composition and film thickness) and the electrical, optical and morphological properties of these layers has been successfully identified. Layers deposited from targets with 2.0 wt% Al_2O_3 present lower resistivity and higher transmittance than layers deposited from targets with 0.5 wt% Al_2O_3. The film thickness has a stronger influence on the electrical properties than on the optical ones. Layers of 1,025 nm thickness show a resistivity as low as $6.54 \times 10^{-4}\,\Omega$cm and a transmittance of 84%.

The electrochemical corrosion behavior of the samples in NaCl solution has been also studied. For all the samples developed under different process parameters, very low corrosion currents (nanoamperes) and very high corrosion resistances (in the order of $10^7\,\Omega$) were obtained. All the samples showed a very high electrochemical stability, which indicates that the developed AZO coatings are not prone to corrosion degradation in aggressive media. Nevertheless, it was found that small modifications in coating structure, dopant and thickness can influence the electrochemical response of the films in chlorinated media.

Acknowledgments

The authors acknowledge financial support from the European Commission obtained in the IN-LIGHT project (7th Framework Programme, FP7; Grant agreement nr.: 314233) and the ERC 2008 Advanced Grant (INVISIBLE n°. 228144), as well as the from the Spanish Ministry of Science and Innovation obtained in the project CSD2008-00023 FUNCOAT (in frames of the CONSOLIDER INGENIO-2010 program) and the Portuguese Science Foundation (FCT-MEC) through the projects EXCL/CTM-NAN/0201/2012 and PEst-C/CTM/LA0025/2013-14.

References

[1] Pern F J, Glick S H, Li X, Dehart C, Gennett T, Contreras M and Gessert T 2009 *Proc. SPIE* **7412** 74120K
[2] Lin J-C, Peng K-C, Peng I-G and Lee S-L 2009 *Thin Solid Films* **517** 4777
[3] Kim J-H, Lee H, Choi S, Bae K H and Park Y 2013 *Thin Solid Films* **547** 163
[4] Dai H-Q, Xu H, Zhou Y-N, Lu F and Fu Z-W 2012 *J. Phys. Chem.* C **116** 1519
[5] Lin S S, He H P, Ye Z Z, Zhao B H and Huang J Y 2008 *J. Appl. Phys.* **104** 114307
[6] Ginley D S (ed) 2011 *Handbook of Transparent Conductors* (Boston, MA: Springer)
[7] Tun C J, Sheu J K, Pong B J, Lee M L, Lee M Y, Hsieh C K, Hu C C and Chi G C 2006 *IEEE Photon. Technol. Lett.* **18** 274
[8] Lim D G *et al* 2006 *Superlattices Microstruct.* **107** 39
[9] Terheggen M, Heinrich H, Kostorz G, Haug F-J, Zogg H and Tiwari A N 2002 *Thin Solid Films* **403** 212
[10] Fortunato E, Nunes P, Costa D, Brida D, Ferreira I and Martins R 2002 *Vacuum* **64** 233–6
[11] Neves N *et al* 2012 *J. Eur. Ceram. Soc.* **32** 4381–91
[12] O'Brien J and Kelly P J 2001 *Surf. Coat. Technol.* **142** 621
[13] Welzel T, Kleinhempel R, Dunger T and Richter F 2009 *Plasma Process. Polym.* **6** S331
[14] Okoshi M, Higashikawa K and Hanabusa M 2001 *Jpn. J. Appl. Phys.* **1287** 40
[15] Szyszka B *et al* 2003 *Thin Solid Films* **179** 442
[16] Chen M, Pei Z L, Sun C, Wen L S and Wang X 2001 *Mater. Lett.* **194** 48
[17] Minami T, Minamino Y, Ida S and Miyata T 2002 *Thin Solid Films* **92** 416
[18] Marotti R E *et al* 2008 *Thin Solid Films* **1077** 517
[19] Suzuki K 1999 *Thin Solid Films* **8** 351
[20] Cebulla R, Werndt R and Ellmer K 1998 *J. Appl. Phys.* **1087** 83
[21] Garcia-Garcia J *et al* 2011 *IEEE Trans. Plasma Sci.* **39** 1983–9
[22] Koidis K *et al* 2010 *Phys. Status Solidi* A **207** 1581–5
[23] Climent-Font A, Pászti F, García G, Fernández-Jiménez M T and Agulló F 2004 *Nucl. Instrum. Methods Phys. Res.* B **219** 400
[24] Kotai E 1994 *Nucl. Instrum. Methods Phys. Res.* B **85** 588
[25] Mayer M 1997 *SIMNRA User's Guid* (Germany: Max-Planck-Institut fur Plasmaphysik)
[26] G-Berasategui E, Zubizarreta C, Ruiz de Gopegui U and Barriga J 2012 *Nanosci. Nanotech. Lett.* **4** 1–5
[27] Kim K H, Park K C and Ma D Y 1997 *J. Appl. Phys.* **81** 7764
[28] Jeong C, Kim H-S, Chang D-R and Kamisako K 2008 *Jpn. J. Appl. Phys.* **47** 5656
[29] Cullity B D 1978 *Elements of X-ray Diffraction* (Boston, MA: Addison-Wesley) p 102
[30] Saito N and Igasaki Y 2001 *Appl. Surf. Sci*. **169** 349
[31] Lupan O, Chow L, Shishiyanu S, Monaico E, Shishiyanu T, Şontea V, Roldan Cuenya B, Naitabdi A, Park S and Schulte A 2009 *Mater. Res. Bull.* **44** 63
[32] Takeda H *et al* 2009 *Thin Solid Films* **517** 3048–52
[33] Hamberg I and Granqvist C G 1986 *J. Appl. Phys.* **60** 123
[34] Pankove J I 1976 *Optical Processes in Semiconductor* (New York: Dover)
[35] Burstein E 1954 *Phys. Rev.* **93** 632
[36] Moss T S 1954 *Proc. Phys. Soc. London* B **67** 775
[37] Mondal S, Bhattacharya S and Mitra P 2013 *Adv. Mater. Sci. Eng.* **2013** 6
[38] Tseng Z-L, Kao P-C, Chen Y-C, Juang Y-D, Kuo Y-M and Chu S-Y 2011 *J. Electrochem. Soc.* **158** J310–5

[39] Islam M M, Ishizuka S, Yamada A, Matsubara K, Niki S, Sakurai T and Akimoto K 2001 *Appl. Surf. Sci.* **4026** 257
[40] Chang J F, Kuo H H, Leu I C and Hon M H 2002 *Sens. Actuators* B **84** 258–64
[41] Owen J I 2011 *Growth, Etching, and Stability of Sputtered ZnO: AI for Thin-film Silicon Solar Cells* (Jülich, Germany: Forschungszentrum)
[42] Kluth O *et al* 1999 *Thin Solid Films* **351** 247–53
[43] Guillén C and Herrero J 2010 *Vacuum* **84** 924–9
[44] Suchea M, Christoulakis S, Katsarakis N, Kitsopoulos T and Kiriakidis G 2007 *Thin Solid Films* **515** 6562–6
[45] Lin S S and Huang J L 2004 *Surf. Coat. Technol.* **185** 222–7
[46] He H P *et al* 2006 *J. Appl. Phys.* 023503 **99**
[47] Fortunato E, Ginley D, Hosono H and Paine D C 2007 *MRS Bull.* **32** 242–7
[48] Lukaszkowicz K, Kwaśny W and Szewczenko J 2011 *J. Achiev. Mater. Manuf. Eng.* **45** 23–9
[49] Bard A J and Faulkner L R 2001 *Electrochemical Methods. Fundamentals and Applications* (New York: John Wiley & Sons)
[50] ASTM G102-89 2010 *Standard Practice of Calculation of Corrosion Rates and Related Information from Electrochemical Measurements* (Pensilvania: ASTM)
[51] Arslan E, Totik Y, Demirci E and Alsaran A 2010 *J. Mat. Eng Perform.* **19** 428–33
[52] Ross Macdonald J 2005 *Impedance Spectroscopy, Theory, Experiment, and Applications* (Hoboken, NJ: John Wiley & Sons) ISBN 0-471-64749-7
[53] MiLosev I, Kosec T, and Strehblow H-H 2008 *Electrochinica Acta* **53** 3547